A New *k*-Distribution Scheme for Clear-Sky Radiative Transfer Calculations in Earth's Atmosphere. Part II: Solar (Shortwave) Heating due to H_2O and CO_2

MING-DAH CHOU,[a] KYU-TAE LEE,[b] IL-SUNG ZO,[b] WEI-LIANG LEE,[c] CHEIN-JUNG SHIU,[c] AND JOON-BUM JEE[d]

[a] *Department of Atmospheric Sciences, National Central University, Taoyuan, Taiwan*
[b] *Department of Atmospheric and Environmental Sciences, Gangneung-Wonju National University, Gangneung, South Korea*
[c] *Research Center for Environmental Changes, Academia Sinica, Taipei, Taiwan*
[d] *Research Center for Atmospheric Environment, Hankuk University of Foreign Studies, Yongin, South Korea*

(Manuscript received 11 September 2020, in final form 28 May 2021)

ABSTRACT: A new *k*-distribution scheme without the assumption of the correlation between the absorption coefficients at different pressures is developed for solar heating due to water vapor and CO_2. Grouping of spectral points is based on the observation that radiation at spectral points with a large absorption coefficient is quickly absorbed to heat the stratosphere, and the heating below is attributable to the absorption of the solar radiation at the remaining spectral points. By grouping the spectral points with a large absorption coefficient at low pressures, the range of the absorption coefficient of the remaining spectral points is narrowed, and the *k*-distribution approximation can be accurately applied to compute solar heating in both the stratosphere and troposphere. Grouping of the spectral points is based on the absorption coefficient at a couple of reference pressures where heating is significant. With a total number of 52 spectral groups in the water vapor and CO_2 bands, fluxes and heating rates were calculated for various solar zenith angles in some typical and sampled atmospheres in diverse climatic regimes and seasons. The maximum heating rate difference between the *k*-distribution and line-by-line calculations is $<0.09\,\mathrm{K\ day^{-1}}$ for water vapor and $<0.2\,\mathrm{K\ day^{-1}}$ for CO_2. The difference in the surface radiation is $\sim 1.4\,\mathrm{W\,m^{-2}}$ for water vapor and $0.6\,\mathrm{W\,m^{-2}}$ for CO_2, while it could increase to $2.6\,\mathrm{W\,m^{-2}}$ due to overlapping absorption. These results can be improved by increasing the number of spectral groups at the expense of computational economy.

KEYWORDS: Gaseous absorption; Radiative transfer; Parameterization

1. Introduction

Computational efficiency has always been an issue in determining solar heating in an absorbing/scattering atmosphere in an atmospheric model, and this is dictated in part by the number of terms needed to compute the gaseous absorption. Within a spectral range that spans an entire water vapor or CO_2 absorption band in the solar spectral region, the magnitude of the absorption coefficient might vary by more than 10 orders of magnitude, and highly simplified radiative transfer schemes must be used to reduce the computational burden. One of the most widely used approaches to expediting the computation is the application of the *k*-distribution approximation (Ambartzumian 1936; Arking and Grossman 1972). This approximation assumes that the spectral points with a similar absorption coefficient in an atmospheric layer can be treated as a single spectral point in all other atmospheric layers. Thus, all points in a spectral band are sorted into a limited number of groups, and each group is treated as monochromatic. As a result, the computation burden is greatly reduced.

Uncertainties in radiative flux calculations due to this approximation arise from the fact that the absorption coefficient is a function of pressure and temperature, and spectral points with a similar absorption coefficient in an atmospheric layer might become dispersed in a distant layer where the pressure is greatly different. This problem can cause calculations of absorption in distant layers to be inaccurate because the absorption coefficients in a spectral group are no longer tightly packed together. A widely used approach to cope with this issue is the application of the correlated *k*-distribution approximation, which assumes that the distributions of the absorption coefficient at different pressures and temperatures are highly correlated (e.g., Goody et al. 1989; Lacis and Oinas 1991; Fu and Liou 1992; Mlawer et al. 1997; Nakajima et al. 2000). Accumulated *k*-distribution functions at a set of pressures and temperatures are computed for a spectral band. Spectral points in a given interval of the accumulated *k*-distribution function are assumed to be identical regardless of pressure and temperature. This approximation can be justified if the atmospheric layers and, hence, pressures are not far apart.

In the thermal infrared [longwave (LW)], the correlated *k*-distribution approximation has been demonstrated to be efficient in flux and cooling rate calculations for the Earth atmosphere (e.g., Fu and Liou 1992; Mlawer et al. 1997). The major reason that the correlated *k*-distribution approximation works well in the LW is that the cooling is primarily contributed from nearby layers, and the distant layers are of secondary importance (Wu 1980; Chou and Kouvaris 1986).

Specifically, as concerns the application of the correlated *k*-distribution approximation to the LW and shortwave (SW), the difference is in the source of radiation; the former comes from the emission of the atmosphere and the surface, whereas

Denotes content that is immediately available upon publication as open access.

Corresponding author: Wei-Liang Lee, leelupin@gate.sinica.edu.tw

DOI: 10.1175/JAS-D-20-0278.1

the latter is the solar radiation incident at the top of the atmosphere (TOA). The absorption of the solar radiation incident at TOA is quickly saturated in the stratosphere at those spectral points near the centers of strong absorption lines. The implication is that distant layers high in the stratosphere have a significant impact on the heating of the troposphere. However, the correlation of k distributions between layers in the stratosphere and troposphere is weak. (This view is to be elaborated later).

The k distribution without the correlation assumption has also been applied to the solar near-infrared (Chou and Lee 1996; Chou and Suarez 1999; Fomin and Correa 2005). Chou and Lee (1996) assumed a single set of the k-distribution function throughout an inhomogeneous atmosphere, which were computed at a pair of reference pressure and temperature corresponding to the height where heating is the most prominent. The absorption coefficient at other pressures and temperatures were extrapolated from the reference pressure and temperature using the ''wing scaling,'' assuming the dominance of the wings of absorption lines on fluxes and heating rates. This wing scaling of the k-distribution method is computationally very fast and can compute accurately the heating rate in the troposphere and lower stratosphere. However, the heating rate error increases in the upper stratosphere. Fomin and Correa (2005) developed an innovative k-distribution scheme for defining the spectral groups and the equivalent absorption coefficient for each group. The vertical profile of the equivalent absorption coefficient was derived by requiring the downward flux in a spectral group to be identical with the line-by-line (LBL) calculations at all atmospheric levels. This scheme is very fast with reasonably high accuracy in solar flux and heating rate calculations.

In Part I of a new k-distribution scheme, Chou et al. (2020) demonstrated that the new scheme without the correlated k-distribution assumption can efficiently compute LW fluxes and cooling rates. In this study, we extend this new scheme to the solar radiative transfer calculations. Unlike the pressure scaling of the absorption coefficient, as in the scheme of Chou and Lee (1996), this new k-distribution scheme can compute accurately solar heating not only in the troposphere but also in the stratosphere.

Section 2 provides information on the LBL method, the division of the SW spectrum, and the sample atmospheres for flux and heating rate calculations. Section 3 formulates the basic equations and defines some relevant parameters of the new k-distribution scheme. Section 4 details the method of the construction of the k-distribution function and the derivation of the equivalent absorption coefficient. Section 5 validates the k-distribution scheme by comparing flux and heating rate calculations with the LBL calculations. Concluding remarks are given in section 6.

2. Line-by-line calculations, spectral bands, and sample atmospheres

The k-distribution parameterization is based on detailed LBL calculations of fluxes and heating rates. Our LBL calculations of the absorption coefficient (Chou and Kouvaris 1986) use the Air Force Geophysical Laboratory 2012 edition of the molecular absorption parameters [High-Resolution Transmission 2012 (HITRAN2012); Rothman et al. 2013]. The molecular line shape is assumed to follow the Voigt function. Following Clough et al. (1992) and Mlawer et al. (1997), the absorption coefficient at wavenumbers $> 25\,\mathrm{cm}^{-1}$ from the line center is set to zero, which is equivalent to a line-cutoff of $25\,\mathrm{cm}^{-1}$. The absorption coefficient is computed at spectral intervals of $0.001\,\mathrm{cm}^{-1}$ throughout the atmosphere. In the middle and upper stratosphere, the Doppler broadening of the width of an absorption line is independent of pressure and increases linearly with wavenumber. Within the temperature range of Earth's atmosphere, the Doppler line half-width is $>0.001\,\mathrm{cm}^{-1}$ in the solar near-infrared for both water vapor and CO_2, which is greater than the pressure-broadened line half-width. Therefore, the spectral interval of $0.001\,\mathrm{cm}^{-1}$ is smaller than the Voigt line half-width. Further, we used the spectral resolution of $0.002\,\mathrm{cm}^{-1}$ to test the flux and heating rate differences between the spectral resolutions of 0.001 and $0.002\,\mathrm{cm}^{-1}$ in LBL calculations and found the differences are negligible. Thus, the use of $\delta\nu = 0.001\,\mathrm{cm}^{-1}$ is adequate for calculating flux and heating rate due to water vapor and CO_2 in the solar infrared.

Similar to Chou and Suarez (1999), the solar spectrum between $0.7\,\mu\mathrm{m}$ ($14\,290\,\mathrm{cm}^{-1}$) and $10\,\mu\mathrm{m}$ ($1000\,\mathrm{cm}^{-1}$) is divided into 3 bands. Table 1 shows the spectral ranges of the three bands. The spectral distribution of the extraterrestrial solar radiation is taken from the 2000 version of the American Society for Testing and Materials (ASTM) Standard Extraterrestrial Spectrum Reference E-490-00, which has a solar constant of $1366.1\,\mathrm{W\,m}^{-2}$ (https://www.nrel.gov/grid/solar-resource/spectra-astm-e490.html). More recently recommended solar spectral data are available, but it is not expected to impact the conclusion of this study. There are a number of water vapor and CO_2 molecular absorption bands across the solar near-infrared. The overall strength of both water vapor and CO_2 bands increases with decreasing wavenumber. Among the three bands, absorption, or atmospheric heating, is the strongest in band 3. The heating due to CO_2 in band 1 is negligible. Therefore, the k-distribution parameterization of the CO_2 heating only applies to bands 2 and 3.

For clear-sky solar heating, this study does not include contributions from O_2, O_3, and continuum absorption, as well as the H_2O absorption in the spectral region with the wavenumber $> 14\,290\,\mathrm{cm}^{-1}$. Oxygen is a minor contributor to solar heating. The k-distribution scheme of this study can be similarly extended to cover the O_2 bands. However, the O_2 absorption is confined to a few narrow bands, and the spectral bands given in Table 1 have to be repartitioned when O_2 absorption is included and the k-distribution approximation applied. The O_3 and continuum absorption coefficients are smooth functions of the wavenumber, and each spectral interval can be treated as gray, i.e., the absorption coefficient is not a function of wavenumber. Applications of the k-distribution approximation to the O_3 and continuum absorption are unnecessary. The absorption in the visible region ($25\,000$–$14\,290\,\mathrm{cm}^{-1}$) by H_2O is weak and primarily near

TABLE 1. Spectral bands, the number of g groups M, and the reference pressure p_r. The number M is the result of "best fits" that meets the subjectively imposed accuracy requirements in flux and heating rate parameterizations.

Spectral band	Spectral band (cm^{-1})	M			p_r (hPa)	
		H_2O	CO_2	All	H_2O	CO_2
1	8200–14 290	12	—	12	30, 300	—
2	4400–8200	12	6	18	30, 300	10, 300
3	1000–4400	12	10	22	10, 300	1, 10
All	1000–14 290	36	16	52	—	—

the surface where the pressure range is narrow. It can be treated as gray with the absorption coefficient a simple function of pressure.

Fluxes and heating rate computed using the k-distribution approximation for three atmospheres typical of tropical (TRP), midlatitude summer (MLS), and subarctic winter (SAW) conditions are compared with the LBL calculations. Each atmosphere is divided into 75 layers. The thickness of a layer is constant in pressure, $\Delta p = 24$ hPa, in the troposphere, and constant in $\Delta \log_{10} p = 0.15$, above the tropopause. The temperature and humidity of the three atmospheres are taken from McClatchey et al. (1972), except the specific humidity in the stratosphere is set to 3.25×10^{-6} for the tropical atmosphere, and 4×10^{-6} for the midlatitude summer and subarctic winter atmospheres. The column integrated water vapor amounts are 39.4, 27.9, and 4.3 kg m^{-2}, and the surface temperatures are 300, 294, and 257 K for the TRP, MLS, and SAW atmospheres, respectively. The normal, half, and doubled atmospheric CO_2 concentrations are set to 400, 200, and 800 ppmv; the 400 ppmv CO_2 concentration is the observation in 2014 at Mauna Loa Observatory, Hawaii.

The three typical atmospheres were used for developing the new k-distribution parameterization. For independent validation of the new parameterization, eight atmospheres in four diverse climatic regimes and two seasons (June and December) were sampled from the ERA5 reanalysis (Hersbach et al. 2020). Table 2 demonstrates the four sites where the sample atmospheres are located and the time of the samples. Those samples include the atmospheres in the Atmospheric Radiation Measurement (ARM) Southern Great Plains in June (SGP-J) and December (SGP-D), ARM North Slope of Alaska in June (NSA-J) and December (NSA-D), warm pool western tropical Pacific in June (WTP-J) and December (WTP-D), and cold pool eastern tropical Pacific in June (ETP-J) and December (ETP-D). These samples range from a highly cold and dry atmosphere to a warm and humid atmosphere with the skin temperature differs by 54 K and the column-integrated water vapor amount by a factor of 25.

3. The k-distribution approximation

The downward solar flux at the zenith angle ϕ_o at the pressure level p integrated over a spectral interval $\Delta\nu$ in a nonscattering atmosphere can be expressed as

$$F^{\downarrow}_{\Delta\nu}(p,\mu) = \int_{\Delta\nu} \mu S_\nu e^{-\tau_\nu(p)/\mu}\, d\nu\,, \tag{3.1}$$

where $\mu = \cos(\phi_o)$, S_ν is the incoming extraterrestrial solar radiation, i.e., insolation at the wavenumber ν, $\tau_\nu(p)$ is the optical thickness between TOA and the pressure level p given by

$$\tau_\nu(p) = \int_0^p k_\nu(p',\theta')\left(\frac{du}{dp'}\right) dp'\,, \tag{3.2}$$

where θ is the temperature, k is the absorption coefficient, and u is the amount of an absorber.

In the line-by-line calculation of radiative transfer, fluxes are computed at a large number of spectral points N with a small interval $\delta\nu$. Equation (3.1) is then approximated by

$$F^{\downarrow}_{\Delta\nu}(p,\mu) = \sum_{i=1}^{N} \mu S_i e^{-\tau_i(p)/\mu}\delta\nu\,, \tag{3.3}$$

where the subscript i denotes the spectral point at ν.

To avoid the burdensome line-by-line calculations in shortwave modeling, the k-distribution approximation is applied, which groups together a large number of spectral points with a similar absorption coefficient and treats them as a single spectral point in radiative transfer calculations. Thus, flux calculations are greatly expedited. For each group, hereafter referred to as g group, the total downward flux of those spectral points is given by

$$F^{\downarrow}_{g}(p,\mu) = \sum_{i\in R_g} \mu S_i e^{-\tau_i(p)/\mu}\delta\nu, \quad g = 1, 2, 3, \ldots, M, \tag{3.4}$$

TABLE 2. Locations, time, skin temperature, and column-integrated water vapor amount of the eight sample atmospheres used for independent validation of the k-distribution approximation. The letters J and D indicate the months of June and December, respectively.

Location and month	Lat (°)	Lon (°)	Time and date	Skin temperature (K)	Column H_2O (kg m^{-2})
SGP-J	36.605	263.485	1400 UTC 1 Jun 2018	302.72	42.30
SGP-D	36.605	263.485	0100 UTC 2 Dec 2018	281.16	11.86
NSA-J	71.323	156.609	0700 UTC 11 Jun 2018	274.73	9.95
NSA-D	71.323	156.609	0500 UTC 11 Dec 2014	248.18	1.82
WTP-J	10.000	140.000	2300 UTC 8 Jun 2017	302.62	44.78
WTP-D	10.000	140.000	1100 UTC 10 Dec 2013	301.83	37.40
ETP-J	−10.000	260.000	2300 UTC 3 Jun 2016	299.70	22.87
ETP-D	−10.000	260.000	2200 UTC 28 Dec 2018	295.96	22.45

where M is the number of g groups, and R_g is the set of spectral points that are sorted into the gth group.

In the k-distribution approximation, $F_g^{\downarrow}(p, \mu)$ is treated as monochromatic given by

$$F_g^{\downarrow}(p,\mu) = \mu S_g e^{-\tau_g(p)/\mu}, \quad g = 1, 2, 3, \ldots, M, \tag{3.5}$$

where S_g is the total insolation in the gth group given by

$$S_g = \sum_{i \in R_g} S_i \delta\nu, \tag{3.6}$$

τ_g is the equivalent optical thickness given by

$$\tau_g(p) = \int_0^p k_g(p', \theta') \left(\frac{du}{dp'}\right) dp', \tag{3.7}$$

and k_g is the equivalent absorption coefficient of the gth group. The derivation of $k_g(p, \theta)$ is to be given in section 4.

Using the k-distribution approximation, the total downward solar flux in a band defined by $\Delta\nu$ at p becomes

$$\begin{aligned} F_{\Delta\nu}^{\downarrow}(p,\mu) \approx \sum_{g=1}^{M} F_g^{\downarrow}(p,\mu) &= \sum_{g=1}^{M} \mu S_g e^{-\tau_g(p)/\mu} = S_{\Delta\nu} \sum_{g=1}^{M} \left(\frac{\mu S_g}{S_{\Delta\nu}}\right) e^{-\tau_g(p)/\mu} \\ &= \mu S_{\Delta\nu} \sum_{g=1}^{M} H_g T_g(p,\mu) = \mu S_{\Delta\nu} T_{\Delta\nu}(p,\mu), \end{aligned} \tag{3.8}$$

where $S_{\Delta\nu}$ is the extraterrestrial solar radiation in the band given by

$$S_{\Delta\nu} = \sum_{g=1}^{M} S_g, \tag{3.9}$$

H_g is the flux-weighted k-distribution function defined as

$$H_g = \frac{S_g}{S_{\Delta\nu}}, \tag{3.10}$$

and $T_g(p, \mu)$ is the transmission function between TOA and the pressure level p given by

$$T_g(p,\mu) = e^{-\tau_g(p)/\mu}. \tag{3.11}$$

Finally, the flux-weighted mean transmittance of the spectral band is given by

$$T_{\Delta\nu}(p,\mu) = \sum_{g=1}^{M} H_g T_g(p,\mu). \tag{3.12}$$

It is noted that all of the above equations apply to the k-distribution approximation both with and without the assumption of the correlation of the k-distribution function between atmospheric layers. The difference between them is the definition of the spectral points contained in a given g group, i.e., R_g in Eqs. (3.4) and (3.6). In this study, the spectral points sorted into a given g group, R_g, stays in the same group, i.e., independent of pressure and temperature. Therefore, the equivalent absorption coefficient k_g is derived from the same spectral points throughout the atmosphere. In the correlated k-distribution approximation, on the other hand, a spectral point could be sorted into different g groups at different pressures, and the spectral points contained in a given g group are not identical at different atmospheric layers. It follows that k_g along an atmospheric path are derived from different spectral points in a correlated k-distribution scheme. It is also noted that the weight H_g is computed in this study using Eqs. (3.6) and (3.10), whereas it is specified in the correlated k-distribution approximation (e.g., Fu and Liou 1992; Mlawer et al. 1997).

For a reflecting surface, the reflected radiation can be considered as isotropic, and the diffuse transmittance of a g group between the surface and a pressure level p is given by (e.g., Liou 2002)

$$T_g^f(p) = 2\int_0^1 e^{-[\tau_g(p_s)-\tau_g(p)]/\mu} \mu \, d\mu. \tag{3.13}$$

When the path of the reflected radiation is connected with that of the downward radiation through surface reflection, then the transmittance between TOA and the pressure p can be expressed as

$$\tilde{T}_g(p,\mu) = e_s T_g(p_s,\mu) T_g^f(p), \tag{3.14}$$

where e_s is the surface reflectivity, and $e_s T_g(p_s, \mu)$ is the fraction of the reflected surface radiation.

The equivalent mean transmittance of the band $\Delta\nu$ for the upward radiation at p becomes

$$\tilde{T}_{\Delta\nu}(p,\mu) = \sum_{g=1}^{M} H_g \tilde{T}_g(p,\mu) = \sum_{g=1}^{M} H_g [e_s T_g(p_s,\mu) T_g^f(p)]. \tag{3.15}$$

Finally, the upward flux in $\Delta\nu$ is given by

$$F_{\Delta\nu}^{\uparrow}(p) = \mu S_{\Delta\nu} \tilde{T}_{\Delta\nu}(p) \tag{3.16}$$

and the net downward flux at p is

$$F_{\Delta\nu}^{\text{net}}(p) = F_{\Delta\nu}^{\downarrow}(p) - F_{\Delta\nu}^{\uparrow}(p). \tag{3.17}$$

For the overlapping absorption of gases, random overlapping is assumed, and the multiplication rule is applied. The flux-weighted transmission functions of a band given in Eqs. (3.12) and (3.15) are then approximated by

$$T_{\Delta\nu}(p,\mu) = \prod_j T_{\Delta\nu,j}(p,\mu) = \prod_j \left[\sum_{g=1}^{M_j} H_{g,j} T_{g,j}(p,\mu)\right]$$

for downward flux, (3.18)

$$\tilde{T}_{\Delta\nu}(p,\mu) = \prod_j \tilde{T}_{\Delta\nu,j}(p,\mu) = \prod_j \left\{\sum_{g=1}^{M_j} H_{g,j} [e_s T_{g,j}(p_s,\mu) T_{g,j}^f(p)]\right\}$$

for upward flux, (3.19)

where the subscript j denotes the absorbing gas. Thus, the construction of a k-distribution scheme comes down to the

derivations of the flux-weighted k-distribution function, H_g, defined by Eq. (3.10) and the equivalent absorption coefficient $k_g(p, \theta)$.

4. Construction of the *k*-distribution scheme

a. Selection of reference pressure and temperature

Grouping of spectral points is based on the absorption coefficient k at a set of reference pressure p_r and temperature θ_r. Since k varies with pressure and temperature, by definition the absorption coefficients of the same set of spectral points in a given g group are most packed at (p_r, θ_r) and become dispersed as (p, θ) deviates from (p_r, θ_r). It follows that the equivalent absorption coefficient of the g group can be estimated most accurately at (p_r, θ_r) and less accurately as (p, θ) deviates from (p_r, θ_r). Accordingly, the reference pressure and temperature should be chosen at the height where heating (or cooling in the case of LW radiation), is most prominent (Chou and Arking 1980; Chou et al. 2020; Fomin and Correa 2005). When heating has multiple peaks, more than one set of (p_r, θ_r) may be needed for enhancing the accuracy of the k-distribution approximation.

The solar radiation in the troposphere is highly affected by the radiation in the stratosphere as the source of solar radiation is coming from above. Radiation at spectral points with a large absorption coefficient is quickly absorbed to heat the stratosphere. Therefore, the spectral points with strong absorption in the stratosphere should be excluded in the grouping of spectral points in the troposphere. It follows that at least one set of (p_r, θ_r) should be chosen in the stratosphere for identifying the spectral points with strong absorption in the stratosphere. With the spectral points of strong absorption excluded, the range of k of the remaining spectral points is narrowed, and the equivalent absorption coefficient, k_g, can be more accurately estimated. The heating rate profile varies with atmospheres and the solar zenith angle. Based on the general shape of the heating rate profile, the reference pressures were judiciously selected. The range of pressure in the troposphere is not large, and it requires no more than one reference pressure somewhere in the upper or middle troposphere. The reference pressures of each band and gas are given in Table 1. There are two reference pressures for all bands; one in the stratosphere and the other in the troposphere except the CO_2 band 3 where the heating in the troposphere is very weak. The impact of temperature on the absorption is of secondary importance to the impact of pressure. In this study, we fixed θ_r at 250 K.

b. Grouping of spectral points and derivation of the k-distribution function

For each spectral band, grouping of spectral points is based on the absorption coefficient at the reference pressure and temperature. With the reference pressures selected and the reference temperature fixed at 250 K for a spectral band $\Delta\nu$, the g groups are defined by first specifying the number of the groups M. Those M groups are divided into subgroups corresponding to each of the reference pressures. Following Chou et al. (2020), steps for grouping spectral points are given below:

- Starting from the smallest reference pressure p_{r1}, high spectral resolution absorption coefficients $k_\nu(p_{r1}, \theta_r)$ are computed using the LBL method.
- Initially, use a large number of M, say 20, and divide the range of $\log_{10}[k_\nu(p_{r1}, \theta_r)]$ into M intervals with a constant width

$$\Delta x_\nu(p_{r1}, \theta_r) = \frac{x^{\max}(p_{r1}, \theta_r) - x^{\min}(p_{r1}, \theta_r)}{M}, \tag{4.1}$$

where $x_\nu(p_{r1}, \theta_r) = \log_{10}[k_\nu(p_{r1}, \theta_r)]$, and $x^{\max}$ and $x^{\min}$ are the maximum and minimum of x_ν in the band $\Delta\nu$. By dividing the range of the absorption coefficient into intervals with a constant size of $\Delta\log_{10}[k_\nu(p_{r1}, \theta_r)]$, the g groups have more comparable ranges of transmittance values than if a constant size of $\Delta k_\nu(p_r, \theta_r)$ is used.

- A g group is defined by the upper and lower boundaries of the absorption coefficient $x^{U_j}(p_{r1}, \theta_r)$ and $x^{L_j}(p_{r1}, \theta_r)$, $j = 1, 2, \ldots, M$. It is noted that the heating in the stratosphere associated with the first reference pressure is attributable to the spectral points with the largest absorption coefficient. Therefore, the grouping of spectral points is in descending order of $k_\nu(p_{r1}, \theta_r)$,

$$x^{L_j}(p_{r1}, \theta_r) = x^{U_j}(p_{r1}, \theta_r) - \Delta x_\nu(p_{r1}, \theta_r)$$

and

$$x^{U_1}(p_{r1}, \theta_r) = x^{\max}(p_{r1}, \theta_r),$$
$$x^{L_M}(p_{r1}, \theta_r) = x^{\min}(p_{r1}, \theta_r).$$

- Based on $k_\nu(p_{r1}, \theta_r)$, each spectral point is identified with a g group corresponding to the first reference pressure $g_1(\nu)$, where g_1 is one of the M groups ranging from 1 to M.
- For each one of the M groups, compute the heating rate profiles of all the spectral points ν contained in the group using the LBL method.
- Compute the total heating rate profiles of each of the M groups by summing over all the heating rate profiles of the spectral points contained in the group.
- Identify judiciously the first m_1 groups that have a substantial contribution to the heating at p_{r1}. Thus, grouping of the first m_1 groups is complete with $g_1(\nu)$ identified, where $g_1 = 1, 2, 3, \ldots, m_1$.
- In defining the next m_2 groups associated with the second reference pressure, p_{r2}, the spectral points already identified with the groups of the first reference pressure, i.e., $x_\nu(p_{r1}, \theta_r) > x^{L_{m_1}}(p_{r1}, \theta_r)$, are excluded and there are only $(M - m_1)$ groups left to be defined.
- Compute the absorption coefficient of the remaining spectral points at the second reference pressure $k_\nu(p_{r2}, \theta_r)$ using the LBL method. Equation (4.1) becomes

$$\Delta x_\nu(p_{r2}, \theta_r) = \frac{x^{\max}(p_{r2}, \theta_r) - x^{\min}(p_{r2}, \theta_r)}{M - m_1} \tag{4.2}$$

for the second reference pressure. Here $x^{\max}$ and $x^{\min}$ are the maximum and minimum of x_ν in the band $\Delta\nu$ with those spectral points identified with the first m_1 groups excluded. Therefore, each of the $(M - m_1)$ g groups associated with the second reference pressure p_{r2} are defined by the upper and lower boundaries of the absorption coefficient

$$x^{L_j}(p_{r2}, \theta_r) = x^{U_j}(p_{r2}, \theta_r) - \Delta x_\nu(p_{r2}, \theta_r),$$

where $j = 1, 2, \ldots, M - m_1$. It is noted that

$$x^{U_1}(p_{r2}, \theta_r) = x^{\max}(p_{r2}, \theta_r),$$
$$x^{L_{M-m1}}(p_{r2}, \theta_r) = x^{\min}(p_{r2}, \theta_r).$$

It is also noted that $x^{U_1}(p_{r2}, \theta_r) \neq x^{L_{m_1}}(p_{r1}, \theta_r)$ as the reference pressures are different.

- Identify each spectral point with a g group corresponding to the second reference pressure $g_2(\nu)$. Here g_2 is one of the $(M - m_1)$ groups ranging from 1 to $(M - m_1)$.
- For each g_2 group, compute the heating rate profiles of all the spectral ν contained in the group $g_2(\nu)$, using the LBL method.
- The total heating rate profile of the group is then derived by summing over all the heating rate profiles of those spectral points in the group; there are a number of $(M - m_1)$ total heating rate profiles.
- Identify judiciously the first m_2 groups that have a substantial contribution to the heating at p_{r2}.
- The same procedures are repeated for defining the last m_3 g groups if three reference pressures are used. For this case, $m_3 = M - m_1 - m_2$, and

$$\Delta x_\nu(p_{r3}, \theta_r) = \frac{x^{\max}(p_{r3}, \theta_r) - x^{\min}(p_{r3}, \theta_r)}{M - m_1 - m_2}. \tag{4.3}$$

- Compose the grouping of spectral points for the spectral band $\Delta\nu$ by combining the first m_1 group of the $g_1(\nu)$, m_2 group of the $g_2(\nu)$, and m_3 group of the $g_3(\nu)$ for the case of three reference pressures. The composed $g(\nu)$ is R_g in Eq. (3.4).
- The large number of M is reduced and the above steps repeated until errors of fluxes and the heating rate calculated using the new k-distribution scheme are greater than the prespecified accuracies.

It is found that two reference pressures are adequate for accurate computations of fluxes and heating rate in the H_2O and CO_2 bands. It is noted that the spectral heating rate profiles were computed using the MLS atmosphere only for identifying the reference pressures and the number of g groups associated with the reference pressures on which spectral points are grouped, i.e., $g(\nu)$. Other typical atmospheres can also be used for the same purposes. The peak of the heating rate profile shifts up and down with the solar zenith angle only slightly. It does not have much impact on the judiciously and empirically selected reference pressures. Figure 1 is the flowchart demonstrating the grouping of spectral points. It is for the case of three reference pressures, but can also be applied to the case of two reference pressures of this study.

Finally, the flux-weighted k-distribution function H_g is computed from Eqs. (3.6) and (3.10), where the set of spectral points R_g is derived from $g(\nu)$ by composing $g_1(\nu)$ and $g_2(\nu)$ for the case of two reference pressures.

c. Equivalent absorption coefficient and k tables

In addition to the number of g groups M, on which spectral points are grouped, the accuracy of a k-distribution approximation depends strongly on how an equivalent absorption coefficient k_g is derived from a group of k_ν's which differ by many orders of magnitude in a spectral band. For example, the k_ν at (400 hPa, 250 K) in the water vapor band 2 (see Table 1) spans over 2 absorption bands centered at 5300 and 7300 cm^{-1} and ranges by 15 orders of magnitude. If the spectral points are sorted into 15 g groups with a constant $\Delta\log_{10}(k_\nu)$, the k_ν in a g group would range by a factor of 10, or $\Delta\log_{10}(k_\nu) = 1.0$. For atmospheric layers with $p < 400$ hPa, the range of k_ν in a g group is even larger. Because the transmittance is highly nonlinear in k_ν, the equivalent absorption coefficient of a g group k_g cannot be the linear average of the k_ν's of all points in the band $\Delta\nu$ unless the k_ν's are all small and the transmittance can be approximated by a linear function of k_ν.

For a given g group where the absorption coefficient and the optical thickness are small at all spectral points, the transmission function can be linearized, and the equivalent absorption coefficient can be approximated by

$$k_{g,\text{lin}}(p, \theta) = \frac{1}{S_g} \sum_{i \in R_g} S_i k_i(p, \theta) \delta\nu, \tag{4.4}$$

where the subscript lin denotes the linear approximation for the mean absorption coefficient.

With the linearization of the transmission function, the mean absorption coefficient of Eq. (4.4) would overestimate the absorption if the optical thickness is not sufficiently small. Therefore, an empirical adjustment of k_g to a value smaller than k_{lin} is necessary for properly representing the mean absorption/transmission of a g group. Following Chou et al. (2020), a nonlinear mean absorption coefficient smaller than k_{lin} is introduced, which is defined as

$$\log_{10} k_{g,\text{nonlin}}(p, \theta) = \frac{1}{S_g} \sum_{i \in R_g} S_i \log_{10} k_i(p, \theta) \delta\nu \tag{4.5}$$

and the equivalent absorption coefficient is taken as the weighted mean of the linear and nonlinear absorption coefficients,

$$k_g(p, \theta) = w_g k_{g,\text{lin}}(p, \theta) + (1 - w_g) k_{g,\text{nonlin}}(p, \theta), \quad 0 < w_g < 1, \tag{4.6}$$

where the subscript "nonlin" denotes the nonlinear approximation for the mean absorption coefficient, and w_g is the weight that approaches 1 for a small optical thickness and decreases with increasing optical thickness. For a given M, an optimal weight of w_g is chosen that minimizes differences

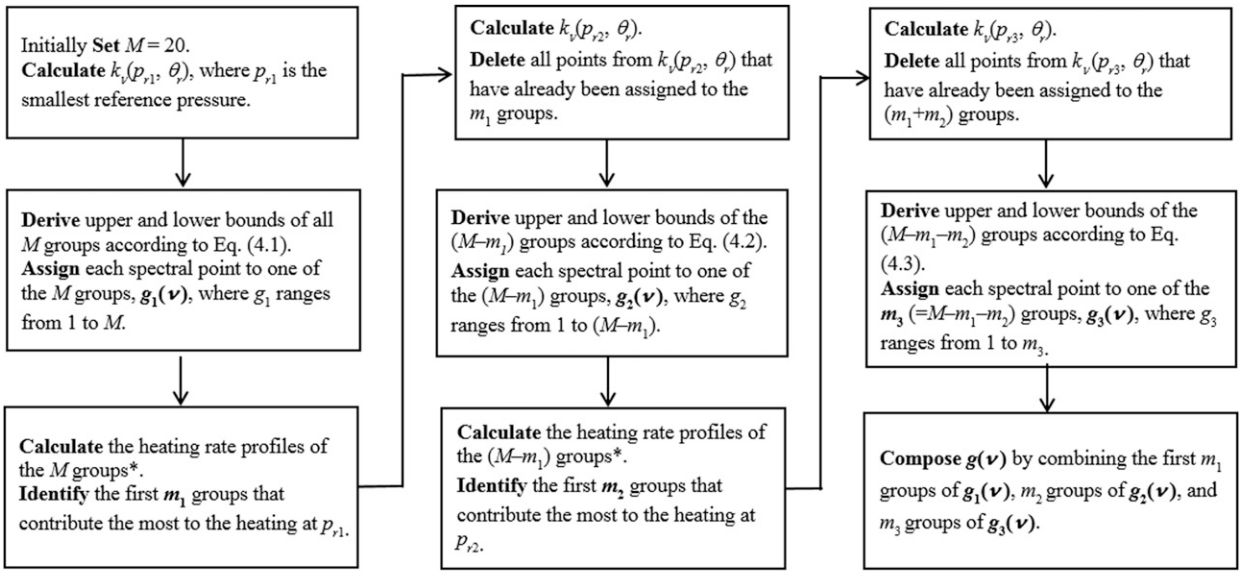

FIG. 1. Grouping of spectral points in each of the bands shown in Table 1. The diagram is for the case of three reference pressures: p_{r1}, p_{r2}, and p_{r3}.

between the k-distribution and LBL calculations of fluxes and the heating rate of the typical tropical, midlatitude summer, and subarctic winter atmospheres with three solar zenith angles, 0°, 60°, and 75°.

Unless the number of g groups, M, is large and $\Delta \log_{10}(k_g)$ is small, the k-distribution approximation has two inherent problems:

1) By using a single value of k_g to represent a wide range of the absorption coefficient in a g group, the nongray radiation of an atmospheric layer is treated as gray radiation. As demonstrated in Chou et al. (2020), the approximation of the nongray radiation of a layer by gray radiation would overestimate absorption when layers are combined in flux calculations. Therefore, the minimization of errors in both the surface flux and the atmospheric heating rate is not feasible. In this study, the weight w_g is chosen that balances the errors in the surface flux and atmospheric heating rate calculations.
2) The monochromatic heating rate profile has a distinct peak that descends in height as the value of k_ν decreases. For a given g group, numerous heating profiles are corresponding to the various values of k_ν at all those spectral points in R_g. When the range of k_ν is large, the range of the heights, where the peaks of the individual heating profiles are located, is also large. Therefore, the heating profile is sharpened when using a single heating profile from $k_g(p, \theta)$ to represent the sum of all heating profiles from $k_\nu(p, \theta)$ in a g group. As a result, the heating rate of a spectral band calculated using $k_g(p, \theta)$ would be oscillatory if the number of the g group, M, is small (Chou and Lee 1996).

In a model spectral band that spans a number of gaseous absorption bands, the absorption coefficient of a large portion of the spectral band is very small that fits Eq. (4.4) for the linearization of the transmission function. Those spectral points are sorted to the last g group, i.e., the Mth g group, and the weight w_g in Eq. (4.6) can be set close to 1.0. By doing so, the range of $\log_{10}(k_\nu)$ of all other spectral points is much reduced, and the efficiency of flux calculations is greatly enhanced. This adjustment in spectral sorting for the Mth g group applies to all of the H_2O and CO_2 bands shown in Table 1.

In this study, the number of g groups M and the weight w_g are chosen by imposing certain requirements on the difference between the k-distribution (KD) and LBL calculations; the results are less sensitive to the weight w_g for a larger number of g groups. For water vapor, the imposed requirement on the difference is $<1.0\,\mathrm{W\,m^{-2}}$ in the surface flux and $<0.05\,\mathrm{K\,day^{-1}}$ in the heating rate from the surface up to 0.01 hPa. For CO_2, the imposed requirement is $<0.5\,\mathrm{W\,m^{-2}}$ in the surface flux, $<0.02\,\mathrm{K\ day^{-1}}$ in the tropospheric heating rate, and $<0.5\,\mathrm{K\,day^{-1}}$ in the stratospheric heating rate.

Using a spectral resolution of $0.001\,\mathrm{cm^{-1}}$, all spectral points in a band $\Delta\nu$ are sorted into the M groups, i.e., $g(\nu)$. Tables of $k_g(p, \theta)$ are then precomputed from Eq. (4.6) using the LBL method. Each table corresponds to a given absorber, spectral band, and g group. There is a total of 52 tables corresponding to the 52 g groups given in Table 1. The size of the tables is 52 pressures × 5 temperatures. The pressure ranges from 0.01 to 1259 hPa with an interval of $\Delta \log_{10}(p) = 0.1$. The temperature ranges by 100 K centered at a temperature profile taken from the mean of the tropical and subarctic winter atmospheres. The $k_g(p, \theta)$ is bilinearly interpolated in $\log_{10}(p)$ and θ from the tables.

5. Validations with line-by-line calculations

By setting the surface reflectivity to 0, i.e., $r_s = 0$, the downward flux and heating rate of some sample atmospheres

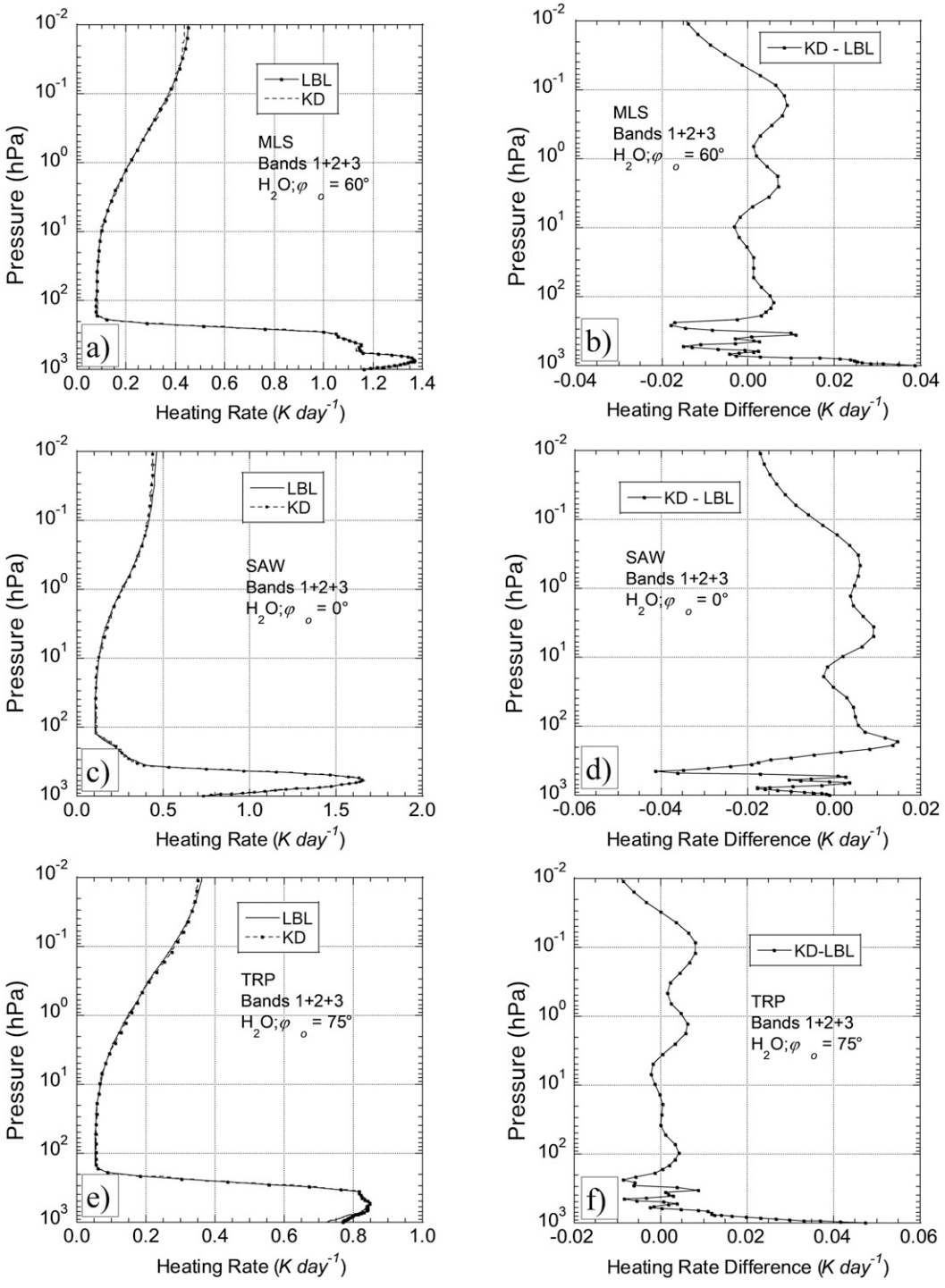

FIG. 2. The total-band water vapor heating rate and heating rate difference between the KD and LBL calculations for (top) a solar zenith angle of 60° in the midlatitude summer atmosphere, (middle) a solar zenith angle of 0° in the subarctic winter atmosphere, and (bottom) a solar zenith angle of 75° in the tropical atmosphere. Here, the total band refers to the sum over bands 1, 2, and 3.

are computed using the k-distribution scheme of Eqs. (3.8) and (3.18), and results are compared with LBL calculations. The equivalent absorption coefficient k_g is interpolated from tables as a function of pressure and temperature precomputed using Eq. (4.6), and the flux-weighted k-distribution function H_g given by Eq. (3.10) is precomputed and specified for each band, gas, and g group. The sample atmospheres include the three typical atmospheres of MLS, TRP, and SAW, two artificial

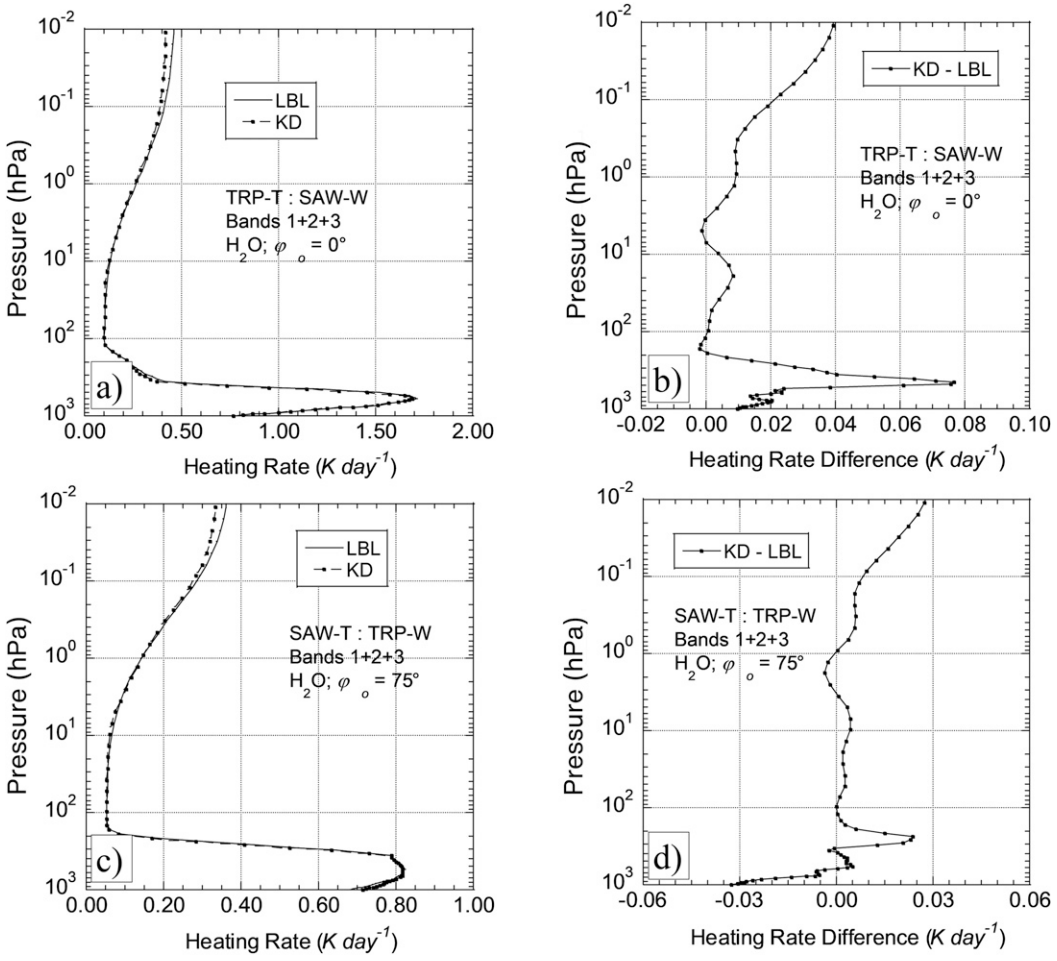

FIG. 3. As in Fig. 2, but for (top) a solar zenith angle of 0° in the TRP-T: SAW-W atmosphere and (bottom) a solar zenith angle of 75° in the SAW-T: TRP-W atmosphere.

atmospheres that mix the temperature and humidity of the TRP and SAW atmospheres, as well as eight atmospheres sampled from four diverse climatic regimes and two seasons.

Figure 2 demonstrates the total heating rate of water vapor in bands 1, 2, and 3 (1000–14 290 cm^{-1}), and the difference between the KD and LBL calculations for three cases: the MLS atmosphere with a solar zenith angle $\varphi_0 = 60°$ (Figs. 2a,b); the SAW atmosphere with $\varphi_0 = 0°$ (Figs. 2c,d); the TRP atmosphere with $\varphi_0 = 75°$ (Figs. 2e,f). The choice of φ_0 for the SAW and TRP cases is to enhance the contrast in the water vapor path; the path-integrated water vapor amount of TRP is 35 times larger than that of SAW. There is a heating peak in the lower troposphere which is due to a large amount of water vapor. Among these three cases, the SAW has the

TABLE 3. The total-band downward surface flux F_s and the difference between the k-distribution (KD) and LBL values, F_s(KD) − F_s(LBL), due to the absorption by water vapor in the three typical and two extreme atmospheres (as described in the text). φ_0 is the solar zenith angle, and F_0 is the incident solar radiation at the top of the atmosphere. The total band refers to the sum over bands 1, 2, and 3. Units are W m^{-2}.

	$\varphi_0 = 0°$, $F_0 = 728.87$ W m^{-2}		$\varphi_0 = 75°$, $F_0 = 188.65$ W m^{-2}	
Atmosphere	F_s(LBL)	F_s(KD) − F_s(LBL)	F_s(LBL)	F_s(KD) − F_s(LBL)
TRP	524.90	−0.64	115.89	−0.95
MLS	539.40	−0.25	119.93	−0.70
SAW	625.71	0.87	147.87	0.05
TRP-T: SAW-W	621.69	0.90	146.72	0.03
SAW-T: TRP-W	532.05	−1.14	117.84	−0.98

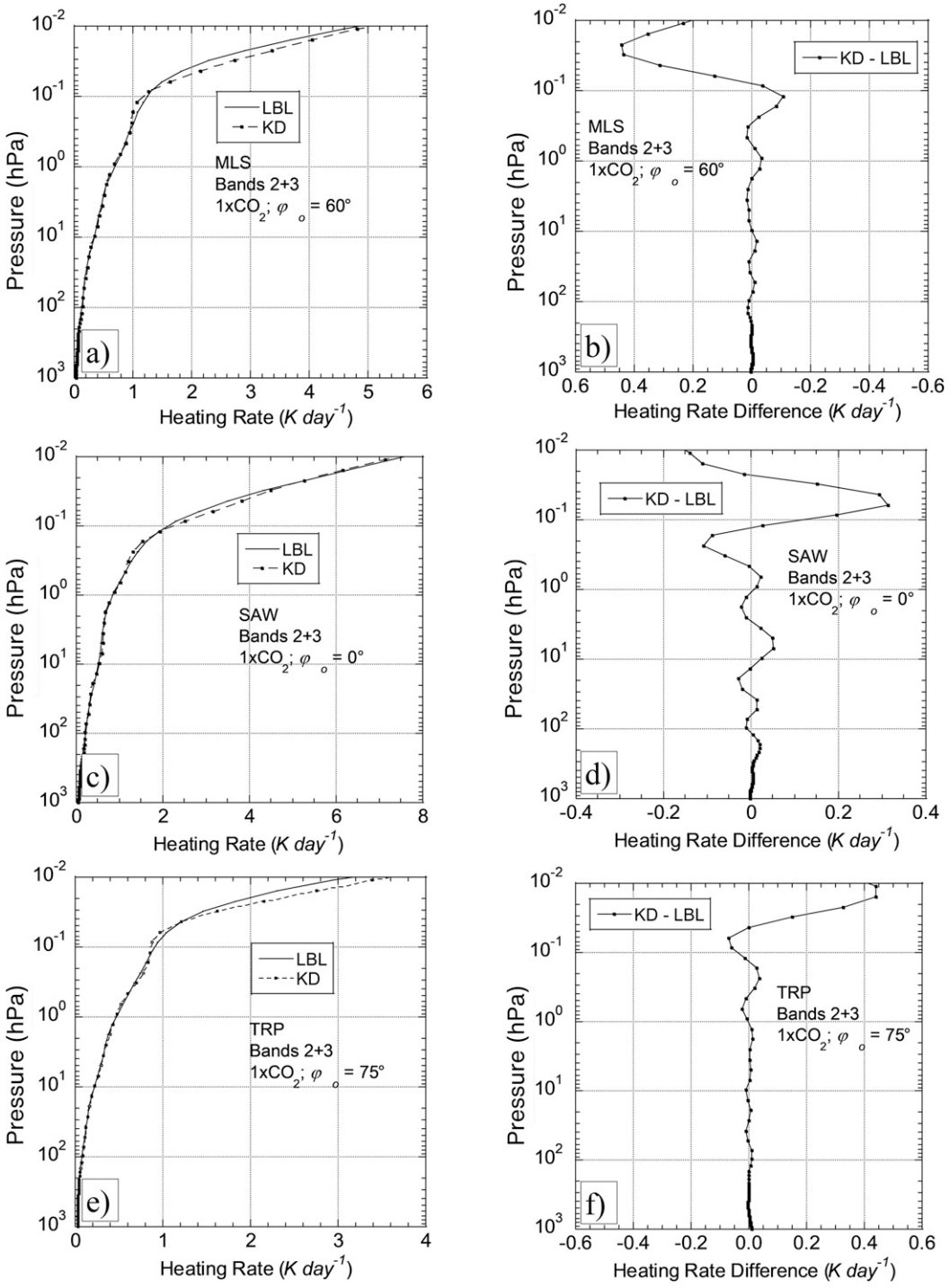

FIG. 4. As in Fig. 2, but for the total-band CO_2 heating rate and heating rate difference. The atmospheric CO_2 concentration is set to 400 ppmv. Here, the total band refers to the sum over bands 2 and 3.

largest heating in the lower troposphere because of the largest solar radiation incident at TOA. The maximum difference in the heating rate between KD and LBL is <0.05 K day^{-1} in the troposphere and <0.02 K day^{-1} in the stratosphere.

In addition to the three typical atmospheres, two artificial atmospheres that mix the TRP atmosphere with the SAW atmosphere are used for independent validation of the *k*-distribution scheme. One has the TRP temperature and SAW water vapor, TRP-T: SAW-W, and the other has the

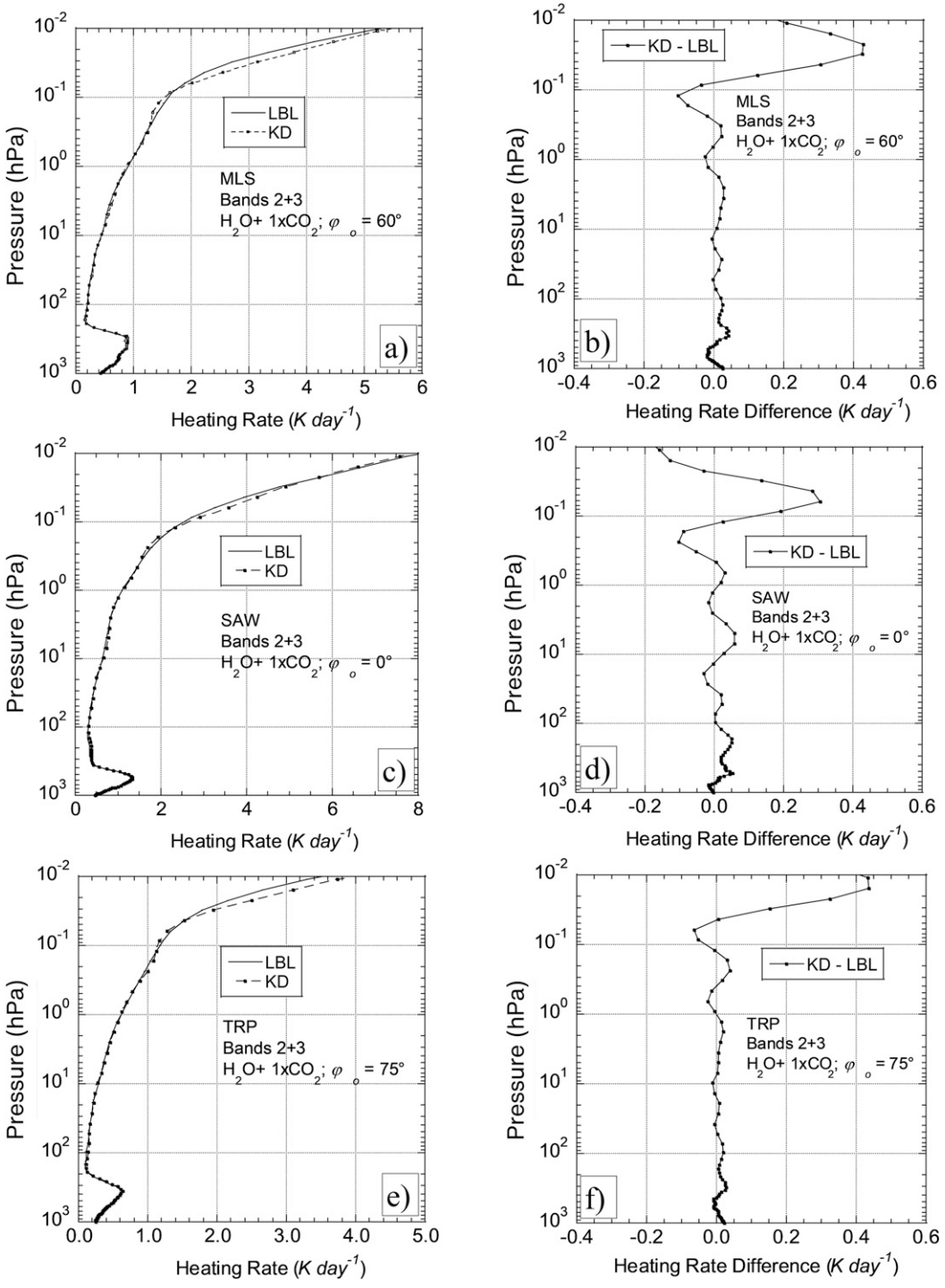

FIG. 5. As in Fig. 4, but for the overlapping absorption due to H_2O and a CO_2 concentration of 400 ppmv.

SAW temperature and TRP water vapor, SAW-T: TRP-W. These two artificial atmospheres differ by a factor of ~10 in the column-integrated water vapor (0.34 vs 4.0 g cm^{-2}) and by 43K in the surface temperature (257 vs 300 K). Figures 3a and 3b demonstrate the heating rate and the heating rate difference between the KD and LBL for the case TRP-T: SAW-W with $\varphi_0 = 0°$, respectively, whereas Figs. 3c and 3d are the case SAW-T: TRP-W with $\varphi_0 = 75°$. The choice of the two solar zenith angles, $\varphi_0 = 0°$ and 75°, is to enhance the difference in the path-integrated water vapor amount between these two artificial atmospheres by a factor of 40. The heating rate difference between the KD and LBL is <0.08 K day^{-1} for

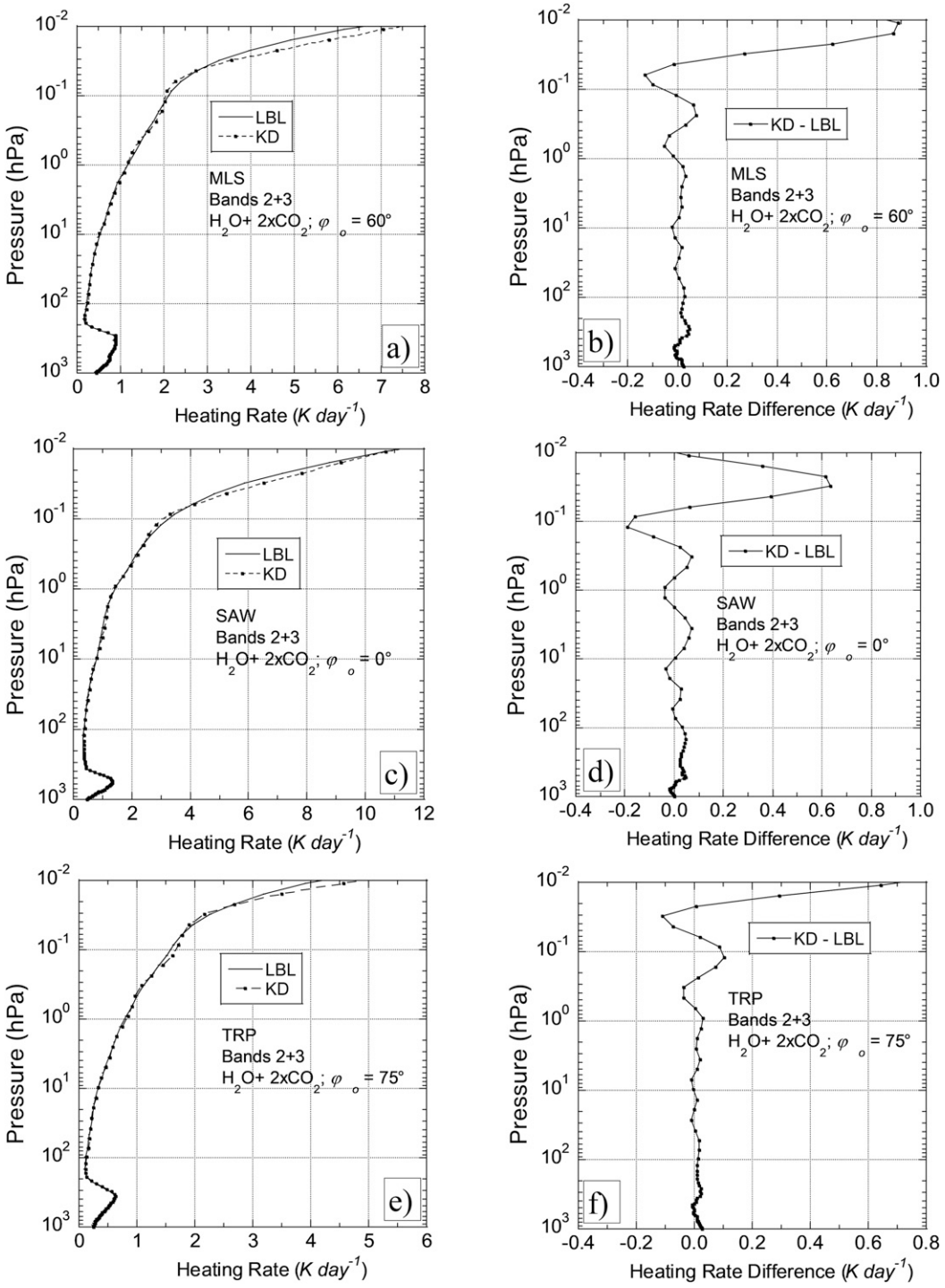

FIG. 6. As in Fig. 5, but for the overlapping absorption due to H_2O and a doubled CO_2 concentration of 800 ppmv.

both cases. Table 3 demonstrates the downward surface radiation F_s and the difference in the downward surface radiation between KD and LBL, $F_s(\mathrm{KD}) - F_s(\mathrm{LBL})$, for the three typical and two extreme atmospheres, as well as two solar zenith angles, 0° and 75°. The difference in the downward surface radiation is $<1.2\ \mathrm{W\,m^{-2}}$.

Figure 4 demonstrates the total heating rate in bands 2 and 3 ($1000–8200\ \mathrm{cm^{-1}}$), of a normal CO_2 concentration of 400 ppmv ($1 \times CO_2$) and the difference between the KD and LBL for the same three cases of the typical atmospheres as Fig. 2: the MLS atmosphere with $\varphi_0 = 60°$, the SAW atmosphere with $\varphi_0 = 0°$, and the TRP atmosphere with $\varphi_0 = 75°$. As revealed in the

TABLE 4. The total-band downward surface flux F_s and the difference between the KD and LBL values ΔF_s [$=F_s(\text{KD}) - F_s(\text{LBL})$], due to the absorption by CO_2. The cases ($0.5 \times CO_2$), ($1 \times CO_2$), and ($2 \times CO_2$) refer to the CO_2 concentrations of 200, 400, and 800 ppmv, respectively. φ_0 is the solar zenith angle. The total band refers to the sum over bands 2 and 3. Units are W m^{-2}. The downward solar flux at the top of the atmosphere is 286.45 W m^{-2} for $\varphi_0 = 0°$.

	$\varphi_0 = 0°$, $0.5 \times CO_2$		$\varphi_0 = 0°$, $1 \times CO_2$		$\varphi_0 = 0°$, $2 \times CO_2$	
Atmosphere	F_s(LBL)	ΔF_s	F_s(LBL)	ΔF_s	F_s(LBL)	ΔF_s
TRP	274.89	−0.38	272.20	−0.16	269.02	−0.28
MLS	274.93	−0.39	272.25	−0.17	269.07	−0.27
SAW	275.29	−0.52	272.67	−0.30	269.60	−0.29
	$\varphi_0 = 75°$, $0.5 \times CO_2$		$\varphi_0 = 75°$, $1 \times CO_2$		$\varphi_0 = 75°$, $2 \times CO_2$	
	F_s(LBL)	ΔF_s	F_s(LBL)	ΔF_s	F_s(LBL)	ΔF_s
TRP	69.71	−0.07	68.68	−0.30	67.50	−1.02
MLS	69.72	−0.07	68.70	−0.29	67.53	−0.98
SAW	69.86	−0.08	68.87	−0.22	67.75	−0.75

figure, the CO_2 solar heating in the stratosphere is very large, greater than 7 K day^{-1} at 0.01 hPa for $\varphi_0 = 0°$, but insignificant in the troposphere. Band 3 contributes to most of the heating in the stratosphere. The heating rate difference between the KD and LBL is generally <0.2 K day^{-1} in the stratosphere, except in the upper stratosphere where the maximum is 0.45 K day^{-1}. In the troposphere, the difference is <0.03 K day^{-1}.

Figure 5 demonstrates the total-band heating rate and heating rate difference due to the overlapping absorption of water vapor and the normal CO_2 concentration of 400 ppmv for the same three cases as in Fig. 4. Since the *k*-distribution parameterization for CO_2 does not apply to band 1, the results demonstrated in the figure cover only bands 2 and 3. For the overlapping absorption, the transmission function is computed from Eq. (3.18). The maximum heating occurs in the upper stratosphere in all three cases. It reaches 8 K day^{-1} for the case of $\varphi_0 = 0°$. By comparison with Fig. 4, the large heating in the stratosphere is primarily due to CO_2. There is also a heating peak in the middle troposphere (300–600 hPa) ranging from 0.6 to 1.6 K day^{-1}. The tropospheric heating is mostly due to water vapor. The heating rate difference between the KD and LBL is <0.05 K day^{-1} in the troposphere and <0.1 K day^{-1} in the stratosphere, except in the region above the 0.1-hPa level.

In addition to the normal CO_2 concentration of 400 ppmv, the new *k*-distribution scheme is also validated with a reduced CO_2 concentration of 200 ppmv ($0.5 \times CO_2$) and a doubled CO_2 concentration of 800 ppmv ($2 \times CO_2$). Figure 6 is the same as Fig. 5 for the total-band (bands 2 and 3) heating rate and heating rate difference due to the overlapping absorption of water vapor and CO_2, except for a doubled CO_2 concentration of 800 ppmv. Compared with Fig. 5, the heating increases in the stratosphere due to a doubled CO_2 but remains nearly unchanged in the troposphere because of the weak CO_2 heating. The difference in the heating between the KD and LBL also increases in the stratosphere due to a doubled CO_2 but remains nearly unchanged in the troposphere. For the case of the reduced CO_2 concentration of 200 ppmv, the results are smaller than those shown in Figs. 5 and 6 (not demonstrated in the figures).

Table 4 demonstrates the downward surface flux F_s and the difference between the KD and LBL values ΔF_s due to the absorption by CO_2 in bands 2 and 3 for the solar zenith angles of 0° and 75°. The difference in the downward surface radiation is only ~0.5 W m^{-2}, except for the cases of a doubled CO_2 and a solar zenith angle of 75° which have a difference of ~1.0 W m^{-2}. Table 5 is the same as Table 4, except for the overlapping absorption of water vapor and

TABLE 5. As in Table 4, but for the overlapping absorption of water vapor and CO_2.

	$\varphi_0 = 0°$, $0.5 \times CO_2$		$\varphi_0 = 0°$, $1 \times CO_2$		$\varphi_0 = 0°$, $2 \times CO_2$	
Atmosphere	F_s(LBL)	ΔF_s	F_s(LBL)	ΔF_s	F_s(LBL)	ΔF_s
TRP	156.44	−2.23	155.19	−2.30	153.51	−2.39
MLS	162.05	−2.09	160.74	−2.15	158.99	−2.22
SAW	201.90	−1.87	200.22	−1.87	198.01	−1.80
	$\varphi_0 = 75°$, $0.5 \times CO_2$		$\varphi_0 = 75°$, $1 \times CO_2$		$\varphi_0 = 75°$, $2 \times CO_2$	
	F_s(LBL)	ΔF_s	F_s(LBL)	ΔF_s	F_s(LBL)	ΔF_s
TRP	33.27	−0.93	32.84	−1.03	32.28	−1.30
MLS	34.73	−0.81	34.27	−0.91	33.69	−1.20
SAW	44.77	−0.52	44.16	−0.59	43.42	−0.87

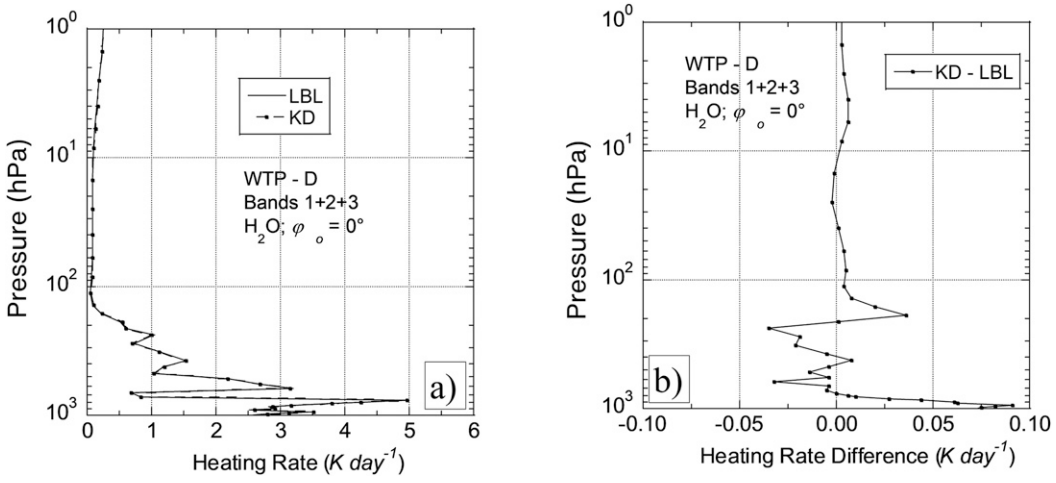

FIG. 7. As in Fig. 2, but for a solar zenith angle of 0° in the western tropical Pacific in December (WTP-D) atmosphere.

CO_2. The atmospheres with a doubled CO_2 and $\varphi_0 = 0°$ have the largest difference of 2.4 W m^{-2} in the downward surface radiation. This difference is substantially larger than that given in Tables 3 and 4 for the absorption due to, respectively, water vapor and CO_2. It is caused by applying the multiplication rule of Eq. (3.18) for the transmission function of overlapping absorption in wide spectral bands. The difference can be reduced by dividing the solar infrared into more than the three bands given in Table 1.

The error in the impact of a doubling of CO_2 induced from using the new *k*-distribution scheme can be readily derived from the data in Table 5. It is the difference in ΔF_s between $2 \times CO_2$ and $1 \times CO_2$. For the case of a solar zenith angle of 75°, the percentage error is large, ~50%, but the absolute error is small, <0.3 W m^{-2}. For the case of a solar zenith angle of 0°, both percentage and absolute errors are insignificant.

The important parameter that affects the climate due to changing CO_2 is the TOA flux but not the surface flux. The TOA flux is important because it is the heating of the Earth-atmosphere system. Surface heating has an impact on the stability of the lower atmosphere near the surface. The extra heat, either positive or negative, is redistributed to the atmosphere through convection. Therefore, the absolute change of the surface heating is important, whereas the relative change is of secondary importance. The error of 0.3 W m^{-2} in the impact of a doubled CO_2 on the surface flux can be considered small.

For independent validation of the new *k*-distribution approximation scheme, we sampled eight atmospheres in four diverse climatic regimes and two seasons (June and December). The locations and the time of the eight sample atmospheres are demonstrated in Table 2. Clear-sky temperatures and humidities of these eight atmospheres were sampled from the ERA5 global reanalysis (Hersbach, et al. 2020). The ERA5 temperature and humidity available to us are defined at 37 pressure levels ranging from 1 to 1000 hPa. In flux and heating rate calculations, we artificially added a layer above 1 hPa and set the temperature and gas concentration to the values at 1 hPa.

Using the KD and LBL schemes, we computed the heating rate profiles and the difference between the KD and LBL values for each of the eight sample atmospheres and three solar zenith angles, $\varphi_0 = 0°$, 60°, and 75°. For a given absorbing gas, we selected from the eight sample atmospheres and the three solar zenith angles the one having the least satisfactory KD-calculated heating rate profile when compared with the LBL

TABLE 6. The maximum difference in the water vapor heating rate profiles between the KD and LBL in the stratosphere (Δh_{stra}) and troposphere (Δh_{trop}), and the difference in the surface flux (ΔF_s) in bands 1–3. φ_0 is the solar zenith angle, and F_0 is the incident solar radiation at the top of the atmosphere. The difference Δ is KD minus LBL. Units are K day^{-1} for the heating rate and W m^{-2} for the flux.

	$\varphi_0 = 0°$, $F_0 = 728.87$				$\varphi_0 = 75°$, $F_0 = 188.65$			
Atmosphere	F_s	Δh_{stra}	Δh_{trop}	ΔF_s	F_s	Δh_{stra}	Δh_{trop}	ΔF_s
SGP-J	518.85	0.01	0.08	−1.33	113.42	0.01	0.06	−1.31
SGP-D	582.85	0.01	0.02	0.40	133.82	0.01	0.01	−0.33
NSA-J	593.24	0.01	0.03	0.64	137.25	0.01	0.02	−0.20
NSA-D	652.60	0.01	0.03	0.94	157.52	0.01	0.01	0.13
WTP-J	518.24	0.01	0.07	−1.24	113.30	0.01	0.06	−1.24
WTP-D	526.91	0.01	0.09	−1.03	115.92	0.01	0.05	−1.11
ETP-J	551.67	0.01	0.08	−0.29	123.68	0.01	0.04	−0.71
ETP-D	549.89	0.01	0.07	−0.34	123.15	0.01	0.04	−0.70

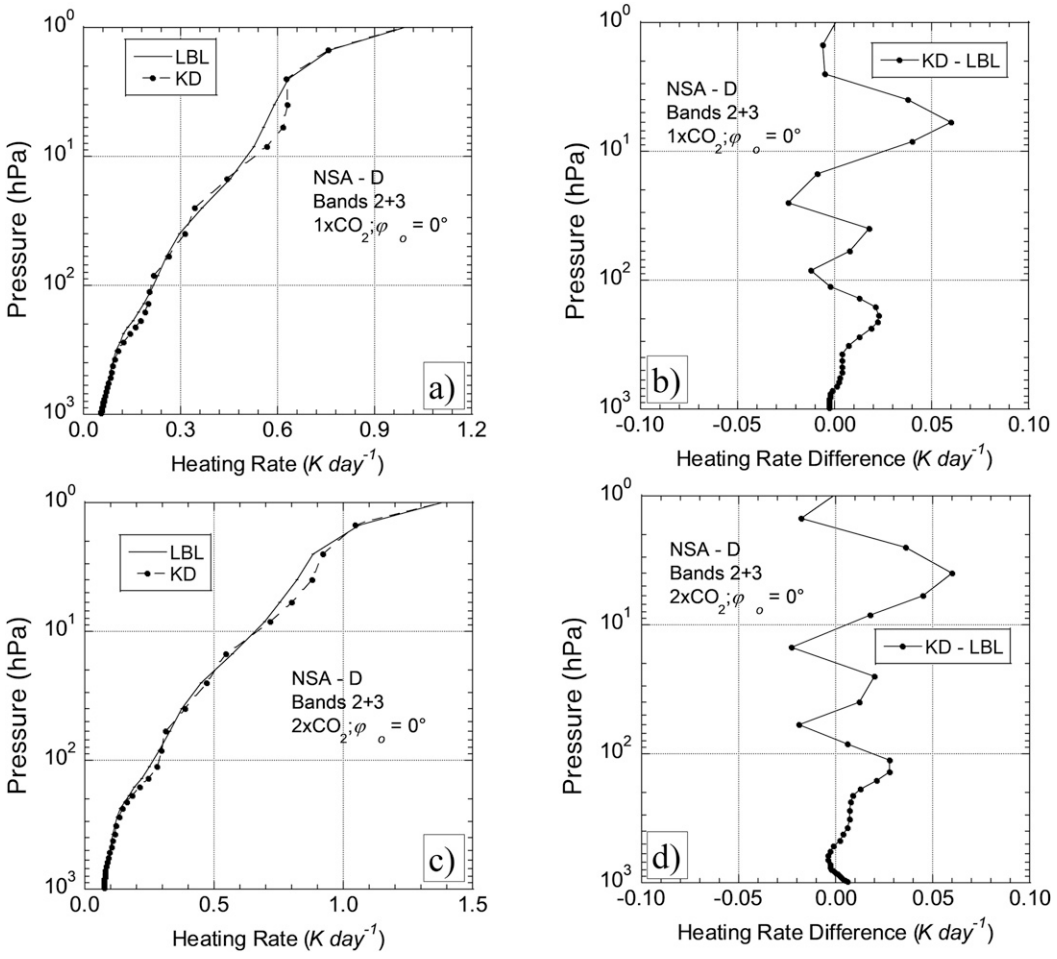

FIG. 8. The total-band heating rates and heating rate differences for a solar zenith angle of 0° in the North Slope of Alaska in December (NSA-D) atmosphere with CO_2 concentrations of (top) 400 and (bottom) 800 ppmv. Here, the total band refers to the sum over bands 2 and 3.

calculations. For water vapor, this case is identified as WTP-D with $\varphi_0 = 0°$, and the results are demonstrated in Fig. 7. The heating rate fluctuates greatly with height in the troposphere, yet the KD can reproduce the fine heating fluctuation. The maximum heating rate of 5 K day^{-1} is located near 750 hPa, and the maximum difference between KD and LBL is 0.09 K day^{-1} at 950 hPa. Table 6 demonstrates the maximum difference in the heating rate profiles between the KD and LBL in the stratosphere (Δh_{stra}) and troposphere (Δh_{trop}), and the difference in the surface flux (ΔF_s) due to the absorption of solar radiation by water vapor in the eight sample ERA5 atmospheres with two solar zenith angles, $\varphi_0 = 0°$ and 75°. The flux and heating rate are the sums over bands 1, 2, and 3. For all of these atmospheres and solar zenith angles, ΔF_s is <1.4 W m^{-2}, Δh_{trop} is <0.09 K day^{-1}, and Δh_{stra} is negligible.

TABLE 7a. As in Table 6, but for the absorption in bands 2 and 3 due to a CO_2 concentration of 200 ppmv.

	$\varphi_0 = 0°$, $F_0 = 286.45$				$\varphi_0 = 75°$, $F_0 = 74.13$			
Atmosphere	F_s	Δh_{stra}	Δh_{trop}	ΔF_s	F_s	Δh_{stra}	Δh_{trop}	ΔF_s
SGP-J	274.87	0.04	0.01	−0.40	69.70	0.01	0.00	−0.10
SGP-D	275.09	0.04	0.02	−0.47	69.78	0.01	0.00	−0.10
NSA-J	275.06	0.03	0.02	−0.46	69.77	0.01	0.01	−0.10
NSA-D	275.31	0.05	0.02	−0.56	69.75	0.02	0.00	−0.12
WTP-J	274.88	0.04	0.01	−0.40	69.70	0.01	0.00	−0.10
WTP-D	274.87	0.04	0.01	−0.40	69.70	0.01	0.00	−0.10
ETP-J	274.89	0.04	0.01	−0.41	69.71	0.01	0.00	−0.10
ETP-D	274.90	0.04	0.01	−0.41	69.71	0.01	0.00	−0.10

TABLE 7b. As in Table 7a, but for the absorption due to a CO_2 concentration of 400 ppmv.

Atmosphere	$\varphi_0 = 0°$, $F_0 = 286.45$				$\varphi_0 = 75°$, $F_0 = 74.13$			
	F_s	Δh_{stra}	Δh_{trop}	ΔF_s	F_s	Δh_{stra}	Δh_{trop}	ΔF_s
SGP-J	272.33	0.04	0.02	−0.29	68.72	0.01	0.01	−0.34
SGP-D	272.58	0.04	0.02	−0.35	68.83	0.01	0.01	−0.30
NSA-J	272.55	0.03	0.02	−0.34	68.81	0.01	0.01	−0.30
NSA-D	272.85	0.04	0.02	−0.45	68.94	0.01	0.01	−0.28
WTP-J	272.33	0.04	0.02	−0.29	68.73	0.01	0.01	−0.35
WTP-D	272.32	0.04	0.02	−0.29	68.72	0.01	0.01	−0.35
ETP-J	272.35	0.04	0.02	−0.29	68.73	0.01	0.01	−0.35
ETP-D	272.35	0.05	0.02	−0.30	68.74	0.01	0.01	−0.35

For CO_2, the least satisfactory KD-calculated heating rate profile is identified as NSA-D with $\varphi_0 = 0°$, and the results for the normal, doubled, and reduced CO_2 cases are demonstrated in Fig. 8. In those cases, the maximum difference between KD and LBL is ~0.06 K day^{-1} in the stratosphere and ~0.03 K day^{-1} in the troposphere. Table 7 is similar to Table 6, except for the absorption of solar radiation by CO_2. Tables 7a, 7b, and 7c are cases with atmospheric CO_2 concentrations of 200, 400, and 800 ppmv, respectively. Differences in the heating rate and the surface flux are small; Δh_{stra} is <0.06 K day^{-1}, Δh_{trop} is <0.03 K day^{-1}, and ΔF_s is <1.1 W m^{-2}. Table 8 is the same as Table 7, except for the overlapping absorption of water vapor and CO_2. Differences in the heating rate and the surface flux are Δh_{stra} is <0.08 K day^{-1}, Δh_{trop} is <0.09 K day^{-1}, and ΔF_s is <2.6 W m^{-2}.

The results presented above were computed using wide ranges of the absorber amount and solar zenith angle. The path-integrated water vapor amount differs by a factor of 40, and the CO_2 concentration ranges from half, normal, and double of the current value. In addition to the standard atmospheres, the sample atmospheres were randomly selected from diverse climate regimes and seasons. Those results demonstrate that the new *k*-distribution approximation is an accurate scheme for calculations of both stratospheric and tropospheric heating due to water vapor, CO_2, and overlapping absorption of these two gases, all in a computationally efficient way.

6. Concluding remarks

A new *k*-distribution scheme for radiative transfer due to water vapor and CO_2 absorption in the solar spectral region is developed. Two major features of this scheme are the grouping of spectral points and derivation of the equivalent absorption coefficient:

1) In grouping the spectral points of a spectral band, a couple of pressure levels, or reference pressures, where solar heating is substantial are identified. By fixing the temperature at 250 K, the range of the absorption coefficient at a reference pressure k_r is divided into a small number of intervals with a constant $\Delta \log_{10}(k_r)$. A spectral point is identified with a $\log_{10}(k_r)$ interval, or *g* group, according to its $\log_{10}(k_r)$ value. Different from the correlated *k*-distribution approximation, a spectral point can only be identified with the same *g* group in all atmospheric layers.
2) Transmission is a highly nonlinear function of the absorption coefficient, and the equivalent absorption coefficient of a *g* group should be adjusted to a value smaller than the linearly averaged absorption coefficient of all the spectral points in the *g* group. Further, using an equivalent absorption coefficient to represent a group of absorption coefficients is equivalent to approximate nongray radiation by gray radiation, which overestimates absorption when atmospheric layers are combined in flux calculations. For these two reasons, the equivalent absorption coefficient is adjusted empirically to obtain a balanced accuracy between the atmospheric heating rate and the surface radiation.

The incident extraterrestrial solar radiation at spectral points with a large absorption coefficient is quickly absorbed to heat the stratosphere and, hence, does not contribute substantially to the heating of the troposphere. Those spectral points are identified from the absorption coefficient at a low reference pressure chosen in the stratosphere. By excluding

TABLE 7c. As in Table 7a, but for the absorption due to a CO_2 concentration of 800 ppmv.

Atmosphere	$\varphi_0 = 0°$, $F_0 = 286.45$				$\varphi_0 = 75°$, $F_0 = 74.13$			
	F_s	Δh_{stra}	Δh_{trop}	ΔF_s	F_s	Δh_{stra}	Δh_{trop}	ΔF_s
SGP-D	269.49	0.03	0.02	−0.42	67.69	0.02	0.03	−0.91
NSA-J	269.44	0.03	0.03	−0.42	67.67	0.03	0.03	−0.93
NSA-D	269.82	0.06	0.02	−0.48	67.83	0.02	0.02	−0.81
WTP-J	269.17	0.04	0.01	−0.44	67.56	0.02	0.03	−1.08
WTP-D	269.16	0.04	0.01	−0.44	67.55	0.01	0.03	−1.09
ETP-J	269.20	0.04	0.02	−0.44	67.57	0.02	0.03	−1.06
ETP-D	269.20	0.04	0.01	−0.44	67.57	0.02	0.03	−1.06

TABLE 8a. As in Table 7a, but for the overlapping absorption of water vapor and a CO_2 concentration of 200 ppmv.

	$\varphi_0 = 0°$, $F_0 = 286.45$				$\varphi_0 = 75°$, $F_0 = 74.13$			
Atmosphere	F_s	Δh_{stra}	Δh_{trop}	ΔF_s	F_s	Δh_{stra}	Δh_{trop}	ΔF_s
SGP-J	153.74	0.04	0.05	−2.35	32.56	0.02	0.03	−1.03
SGP-D	179.81	0.02	0.04	−1.69	39.23	0.01	0.02	−0.60
NSA-J	184.63	0.03	0.06	−1.65	40.40	0.01	0.02	−0.57
NSA-D	218.54	0.05	0.05	−1.75	49.04	0.02	0.01	−0.48
WTP-J	153.80	0.04	0.08	−2.30	32.59	0.02	0.02	−0.99
WTP-D	156.71	0.04	0.07	−2.25	33.33	0.02	0.02	−0.94
ETP-J	166.07	0.04	0.06	−1.99	35.73	0.02	0.03	−0.78
ETP-D	165.56	0.04	0.06	−2.00	35.61	0.02	0.02	−0.77

those spectral points from a spectral band, the range of the absorption coefficient of the remaining spectral points is narrowed, and the *k*-distribution approximation can be applied to accurately compute fluxes and heating rate in both the stratosphere and the troposphere. For the absorption due to water vapor and CO_2, random overlapping of the absorption is assumed, which is only for clear skies.

The new *k*-distribution scheme is applied to compute fluxes and heating rates in three typical atmospheres, two artificial extreme atmospheres, and eight atmospheres sampled from four diverse climatic regimes and two seasons. With the solar infrared divided into three wide bands as demonstrated in Table 1 and the use of a total of 52 *g* groups in the water vapor and CO_2 bands, the heating rate difference between the *k*-distribution and line-by-line calculations in the spectral region 1000–14 290 cm^{-1} is <0.09 K day^{-1} for water vapor, and <0.2 K day^{-1} for CO_2 except in regions near 0.01 hPa. The difference in the downward surface radiation is <1.4 W m^{-2} for water vapor and <0.6 W m^{-2} for CO_2. With the overlapping absorption of water vapor and CO_2, the difference in heating rate is nearly the same as water vapor in the troposphere and CO_2 in the stratosphere. However, the difference in the downward surface flux increases to 2.6 W m^{-2}. The results are sensitive to the number of *g* groups, which is equivalent to the spectral resolution of the *k*-distribution scheme. Results can be improved by dividing the solar infrared into more than three bands and increasing the number of *g* groups. In summary, this new *k*-distribution scheme demonstrates 1) the stability of the parameterization in light of the wide range of water vapor column amounts and CO_2 amounts, 2) the accurate parameterization of the effect of the overlap of water vapor and CO_2, and 3) the accurate parameterization of both stratospheric and tropospheric heating, all in a computationally efficient way.

The current wide spectral limits used have their limitations. For example, variations in the scattering properties of clouds with wavenumbers are not small in the three wide spectral bands of Table 1, and treatments of the overlapping of cloud scattering with gaseous absorption in cloudy skies can be more accurate by increasing the number of spectral bands. In addition to the issue of the scattering properties of clouds, there is also the issue of overlapping of absorption due to multiple gases. In this study, we used the multiplication rule to compute the mean transmission function of a band [Eqs. (3.18) and (3.19)] in clear skies by assuming the spectral overlapping of the gaseous absorption coefficients is random. For a wide spectral band that encloses at least an entire H_2O or CO_2 absorption band, the assumption of random overlapping of the absorption coefficients would degrade the flux and heating rate calculations. Therefore, a partition of narrower spectral bands than those given in Table 1 is necessary for improving solar heating calculations even in clear skies.

However, there is an ensuing issue on the computational economy when the spectrum is divided into more narrower bands. To reach a similar level of accuracy, the total number of *g* groups, i.e., *M*, of the narrow bands would be larger than that of the broad band, and flux calculations would be more expensive. This is because of the large spectral variation of the absorption coefficient, which is dominated by the absorption coefficient of single molecular lines. If a broad band having an

TABLE 8b. As in Table 7b, but for the overlapping absorption of water vapor and a CO_2 concentration of 400 ppmv.

	$\varphi_0 = 0°$, $F_0 = 286.45$				$\varphi_0 = 75°$, $F_0 = 74.13$			
Atmosphere	F_s	Δh_{stra}	Δh_{trop}	ΔF_s	F_s	Δh_{stra}	Δh_{trop}	ΔF_s
SGP-J	152.51	0.04	0.07	−2.43	32.13	0.02	0.03	−1.13
SGP-D	178.33	0.05	0.04	−1.72	38.70	0.02	0.02	−0.69
NSA-J	183.09	0.04	0.07	−1.66	39.85	0.02	0.02	−0.66
NSA-D	216.71	0.07	0.05	−1.75	48.36	0.02	0.01	−0.55
WTP-J	152.58	0.07	0.08	−2.38	32.17	0.02	0.03	−1.09
WTP-D	155.45	0.04	0.09	−2.32	32.89	0.02	0.03	−1.05
ETP-J	164.71	0.06	0.04	−2.04	35.25	0.02	0.02	−0.88
ETP-D	164.21	0.08	0.05	−2.06	35.13	0.02	0.02	−0.87

TABLE 8c. As in Table 7c, but for the overlapping absorption of water vapor and a CO_2 concentration of 800 ppmv.

Atmosphere	$\varphi_0 = 0°$, $F_0 = 286.45$				$\varphi_0 = 75°$, $F_0 = 74.13$			
	F_s	Δh_{stra}	Δh_{trop}	ΔF_s	F_s	Δh_{stra}	Δh_{trop}	ΔF_s
SGP-J	150.87	0.05	0.06	−2.53	31.59	0.02	0.03	−1.39
SGP-D	176.36	0.04	0.05	−1.72	38.05	0.02	0.02	−0.98
NSA-J	181.05	0.03	0.07	−1.66	39.17	0.02	0.02	−0.96
NSA-D	214.31	0.07	0.04	−1.66	47.54	0.03	0.01	−0.85
WTP-J	150.94	0.07	0.08	−2.47	31.63	0.02	0.03	−1.36
WTP-D	153.77	0.04	0.08	−2.42	32.34	0.02	0.03	−1.32
ETP-J	162.90	0.06	0.07	−2.11	34.65	0.02	0.03	−1.18
ETP-D	162.40	0.05	0.07	−2.12	34.54	0.02	0.02	−1.17

absorption coefficient ranges by an order of 10 is divided into two narrow bands, the sum of the ranges of the absorption coefficient in the two narrow bands should be larger than 10.

The scope of this study is limited to the computation of solar heating in nongray spectral regions where the variation of the absorption coefficient with wavenumber is not smooth and the *k*-distribution (or the correlated *k*-distribution) approximation applies. It does not include the heating due to O_3, the minor heating due to O_2, and the continuum absorption. The O_3 and continuum absorptions are smooth with respect to wavenumber and do not need the application of the new *k*-distribution (or the correlated *k*-distribution) approximation. The new *k*-distribution can be extended to compute the heating in the minor O_2 bands. The scattering due to clouds and aerosols and the Rayleigh scattering are also beyond the scope of this study.

In terms of applications, the correlated *k*-distribution method and the new *k*-distribution method are identical, except the flux-weighted *k*-distribution function [the term H_g in Eq. (3.10)] and the equivalent absorption coefficient [the term k_g in Eq. (3.7)] are precomputed (or specified) differently. Thus, this new *k*-distribution approximation can be used as an option to modify the existing full-scale radiative transfer models, such as the RRTMGP (Pincus et al. 2019) and the model of Li and Barker (2005), which use the correlated *k*-distribution approximation in computing the nongray gaseous absorption.

Acknowledgments. This research was supported by National Research Foundation of Korea Grant from the Korean Government ([the Ministry of Science and ICT (MSIT)] (NRF-2021M1A5A1075532), and the Ministry of Science and Technology, Taiwan, under Contracts MOST 107-2119-M-001-011 and MOST 108-2111-M-001-016. The HITRAN2012 molecular spectroscopic database freely available for use in this research is greatly appreciated. The modern CO_2 in the atmosphere observed at Mauna Loa Observatory was taken from the U.S. Department of Commerce/NOAA website: https://www.esrl.noaa.gov/gmd/dv/iadv/graph.php?code=MLO&program=hats&type=ts. The temperature and humidity data of the eight sample atmospheres were taken from the ERA5 website: https://www.ecmwf.int/en/forecasts/datasets/reanalysis-datasets/era5.

REFERENCES

Ambartzumian, V., 1936: The effect of absorption lines on the radiative equilibrium of the outer layers of the stars. *Publ. Obs. Astron. Univ. Leningrad*, **6**, 7–18.

Arking, A., and K. Grossman, 1972: The influence of line shape and band structure on temperatures in planetary atmospheres. *J. Atmos. Sci.*, **29**, 937–949, https://doi.org/10.1175/1520-0469(1972)029<0937:TIOLSA>2.0.CO;2.

Chou, M.-D., and A. Arking, 1980: Computation of infrared cooling rates in the water vapor bands. *J. Atmos. Sci.*, **37**, 855–867, https://doi.org/10.1175/1520-0469(1980)037<0855:COICRI>2.0.CO;2.

——, and L. Kouvaris, 1986: Monochromatic calculations of atmospheric radiative transfer due to molecular line absorption. *J. Geophys. Res.*, **91**, 4047–4055, https://doi.org/10.1029/JD091iD03p04047.

——, and K.-T. Lee, 1996: Parameterizations for the absorption of solar radiation by water vapor and ozone. *J. Atmos. Sci.*, **53**, 1203–1208, https://doi.org/10.1175/1520-0469(1996)053<1203:PFTAOS>2.0.CO;2.

——, and M. J. Suarez, 1999: A solar radiation parameterization for atmospheric studies. NASA Tech. Memo. NASA/TM-1999-104606, Vol. 15, 38 pp., http://gmao.gsfc.nasa.gov/pubs/docs/Chou136.pdf.

——, J. C.-C. Yu, W.-L. Lee, C.-J. Shiu, K.-T. Lee, I.-S. Zo, J.-B. Jee, and B.-Y. Kim, 2020: A new *k*-distribution scheme for clear-sky radiative transfer calculations in Earth's atmosphere: Part I. Thermal infrared (longwave) radiation. *J. Atmos. Sci.*, **77**, 2237–2256, https://doi.org/10.1175/JAS-D-19-0088.1.

Clough, S. A., M. J. Iacono, and J.-L. Moncet, 1992: Line-by-line calculations of atmospheric fluxes and cooling rates: Application to water vapor. *J. Geophys. Res.*, **97**, 15 761–15 785, https://doi.org/10.1029/92JD01419.

Fomin, B., and M. P. Correa, 2005: A *k*-distribution technique for radiative transfer simulation in inhomogeneous atmosphere: 2. FKDM, fast *k*-distribution model for the shortwave. *J. Geophys. Res.*, **110**, D02106, https://doi.org/10.1029/2004JD005163.

Fu, Q., and K.-N. Liou, 1992: On the correlated *k*-distribution method for radiative transfer in nonhomogeneous atmospheres. *J. Atmos. Sci.*, **49**, 2139–2156, https://doi.org/10.1175/1520-0469(1992)049<2139:OTCDMF>2.0.CO;2.

Goody, R. M., R. West, L. Chen, and D. Crisp, 1989: The correlated-*k* method for radiation calculation in nonhomogeneous atmospheres. *J. Quant. Spectrosc. Radiat. Transfer*, **42**, 539–550, https://doi.org/10.1016/0022-4073(89)90044-7.

Hersbach, H., and Coauthors, 2020: The ERA5 global reanalysis. *Quart. J. Roy. Meteor. Soc.*, **146**, 1999–2049, https://doi.org/10.1002/qj.3803.

Lacis, A., and V. Oinas, 1991: A description of the correlated *k*-distribution method for modeling nongray gaseous absorption, thermal emission, and multiple scattering in vertically inhomogeneous atmospheres. *J. Geophys. Res.*, **96**, 9027–9063, https://doi.org/10.1029/90JD01945.

Li, J., and H. W. Barker, 2005: A radiation algorithm with correlated-*k* distribution. Part I: Local thermal equilibrium. *J. Atmos. Sci.*, **62**, 286–309, https://doi.org/10.1175/JAS-3396.1.

Liou, K.-N., 2002: *An Introduction to Atmospheric Radiation.* 2nd ed. Academic Press, 583 pp.

McClatchey, R. A., R. W. Fenn, J. E. A. Selby, F. E. Volz, and J. S. Garing, 1972: Optical properties of the atmosphere. 3rd ed. AFCRL Rep. 72-0497, 108 pp.

Mlawer, E. J., S. J. Taubman, P. D. Brown, M. J. Iacono, and S. A. Clough, 1997: Radiative transfer for inhomogeneous atmospheres: RRTM, a validated correlated-*k* model for the longwave. *J. Geophys. Res.*, **102**, 16 663–16 682, https://doi.org/10.1029/97JD00237.

Nakajima, T., M. Tsukamoto, Y. Tsushima, A. Numaguti, and T. Kimura, 2000: Modeling of the radiative process in an atmospheric general circulation model. *Appl. Opt.*, **39**, 4869–4878, https://doi.org/10.1364/AO.39.004869.

Pincus, R., E. J. Mlawer, and J. S. Delamere, 2019: Balancing accuracy, efficiency, and flexibility in radiation calculations for dynamical models. *J. Adv. Model. Earth Syst.*, **11**, 3074–3089, https://doi.org/10.1029/2019MS001621.

Rothman, L. S., and Coauthors, 2013: The HITRAN2012 molecular spectroscopic database. *J. Quant. Spectrosc. Radiat. Transfer*, **130**, 4–50, https://doi.org/10.1016/j.jqsrt.2013.07.002.

Wu, M.-L. C., 1980: The exchange of infrared radiative energy in the troposphere. *J. Geophys. Res.*, **85**, 4084–4090, https://doi.org/10.1029/JC085iC07p04084.